Invited Paper

Stable optomechanical Fabry-Pérot architecture in a continuous microwave-to-optical transducer

Maxwell D. Urmey[a,b], Sarang Mittal[a,b], Kazemi Adachi[a,b], Luca G. Talamo[a,b], Sarah Dickson[a,b], Sheng-Xiang Lin[a,b], Robert D. Delaney[a,b], Benjamin M. Brubaker[a,b], Jonathan M. Kindem[a,b], Nicholas E. Frattini[a,b], Konrad W. Lehnert[a,b,c], and Cindy A. Regal[a,b]

[a]JILA, National Institute of Standards and Technology and the University of Colorado, Boulder, Colorado 80309, USA
[b]Department of Physics, University of Colorado, Boulder, Colorado 80309, USA
[c]National Institute of Standards and Technology, Boulder, Colorado 80305, USA

ABSTRACT

A transducer capable of faithfully converting single quanta between microwave and optical frequencies would enable an optical network of superconducting quantum computers. A primary challenge in the ongoing effort to bridge these frequency scales is the detrimental effect that optical photons have on superconducting circuits. This manuscript details the membrane-optomechanical Fabry-Pérot architecture we employ in a high-efficiency electro-optomechanical transducer. We use a chemical bonding process to create an integrated membrane-mirror etalon assembly that is robust against thermal misalignment upon cryogenic cooling. Our choice of input coupling mirror and cavity geometry allow flexible operation of the transducer in the presence of any additional nonidealities in the optical cavity, such as additional scattering loss associated with one mirror. Our transducer is unique in its ability to operate with continuous laser illumination without substantially impacting the superconducting circuitry of the transducer or a superconducting transmon qubit linked to its microwave input. We quantify the effect of laser light on the superconductor, measuring the effective occupancy of the transducer's superconducting circuit with varying optical power to be less than 0.15 photons even at powers greatly exceeding that needed for transducer operation. We also measure the coherence time T_2 of a qubit attached to the transducer for optical readout, and determine that continuous laser pumping of the transducer has no measurable effect.

Keywords: Microwave-to-optical transduction, superconducting-qubit readout, Fabry-Pérot optical cavity, quantum optomechanics, membrane optomechanics, frequency conversion, quantum network

1. INTRODUCTION

Microwave-frequency superconducting circuits are a promising platform for quantum computers.[1] However, the low excitation energy of the microwave photon precludes a quantum network from operating with room-temperature linkages. The higher energy scale of optical photons, on the other hand, is naturally compatible with networking applications.[2] A sufficiently low-noise microwave-to-optical transducer would therefore enable a quantum network of superconducting quantum computers. Promising demonstrations have been accomplished using neutral atoms,[3–6] embedded ions,[7–9] nonlinear materials,[10–14] microwave-frequency optomechanical crystals with piezoelectric material,[15,16] and membrane electro-optomechanics.[17] Piezo-optomechanical transducers have demonstrated transduction of single microwave photons from a transmon qubit,[18] and measured entangled pairs of optical and microwave photons.[19] Bulk nonlinear electro-optic devices have demonstrated input-referred added noise of less than one photon,[20] and have inferred entanglement between continuous fields at the outputs of their device.[21]

However, all platforms suffer from a common challenge: photons from the optical pump necessary to bridge the difference in frequency are sufficiently energetic to disrupt the superconductivity that channels the microwave photons, which would result in substantial noise. The promising results from using the piezo-optomechanical and nonlinear electro-optic were attained by pulsing transducer operation to beat the timescale of the negative

maxwell.urmey@colorado.edu

Quantum Computing, Communication, and Simulation IV, edited by Philip R. Hemmer, Alan L. Migdall, Proc. of SPIE Vol. 12911, 1291109 · © 2024 SPIE
0277-786X · doi: 10.1117/12.3008938

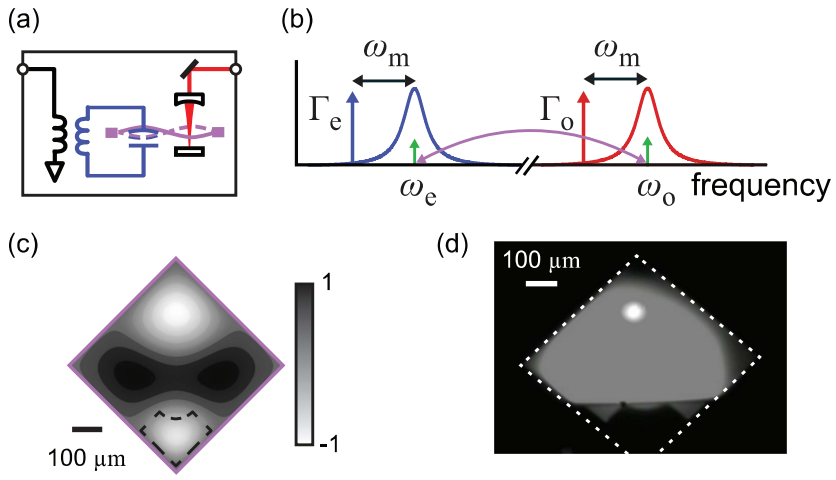

Figure 1. **Transducer operation.** (a) Transducer schematic. A vibrational mode of the silicon nitride membrane (purple) couples to the microwave-frequency LC circuit (blue) and Fabry-Pérot cavity mode (red). (b) Frequency diagram of transducer operation. Optical and microwave pumps are red detuned from the cavity and LC resonance frequencies ω_o and ω_e, respectively, by the mechanical mode frequency ω_m, causing optomechanical and electromechanical damping rates Γ_o and Γ_e, proportional to the respective pump powers. (c) Normalized displacement profile from finite element simulation of the transduction mode. Dashed line indicates position of the capacitor pad.[24] (d) Photograph of the membrane and optical cavity mode in a transducer device operating at mK temperatures in a dilution refrigerator. The membrane is imaged with non-cavity-resonant light from a light-emitting diode, and optical cavity mode is the circular spot in the upper corner. The dashed white line indicates the position of the frame of the membrane, as a guide to the eye. The optical mode intersects the membrane close to the expected position of the antinode of motion.

effects from the optical pump, at the cost of reducing the duty cycle of transducer operation. Low duty cycle pulsed operation greatly reduces the rate of coincidence events needed for intensity correlation experiments to verify the quantum statistics of the transduced signal.

Membrane-based electro-optomechanical transducers offer an alternative that allows for spatial separation of optical and microwave modes.[17,22] Though the MHz-scale mechanical frequency presents an additional challenge because even at millikelvin temperatures it is driven by a thermally occupied environment,[23] we have recently cooled the mechanical mode to its ground state,[24] and transduced the readout pulse of a transmon qubit for measurement using optical heterodyne detection.[25] In this manuscript, we outline the development of the integrated optomechanical cavities with reduced sensitivity to misalignment that enabled these advances. Even when operated continuously, our optical resonator architecture allows transduction with both low laser-induced noise of the microwave circuit[24] and low backaction on a superconducting transmon qubit.[25]

2. MEMBRANE-BASED TRANSDUCER OPERATION

Our transducer consists of an optical Fabry-Pérot cavity and a microwave-frequency LC circuit that are dispersively coupled to the same vibrational mode of a silicon nitride membrane, as illustrated in Fig. 1(a).[17,23,24] We parametrically drive the optical cavity and LC circuit with coherent pumps, red-detuned by the membrane's resonant frequency ω_m from their respective resonant frequencies ω_o and ω_e, in order to enhance a beamsplitter interaction that couples the mechanical mode with the electromagnetic resonator modes, as illustrated in Fig. 1(b). Energy and information is then exchanged between the mechanical oscillator and the optical cavity (LC circuit) at rate Γ_o (Γ_e), proportional to the power of the optical (microwave) pump.[26] An incident signal resonant with one of the electromagnetic resonators is then transduced via the mechanical mode to the other frequency with transduction bandwidth $\Gamma_t = \Gamma_o + \Gamma_e + \gamma_m$, where γ_m is the intrinsic energy loss rate of the mechanical mode. A narrowband signal will be transduced with efficiency $\eta_t = \eta_M \left(4\Gamma_e\Gamma_o/\Gamma_t^2\right)$. The efficiency is maximized at a value of $\eta_M = \epsilon\,(\kappa_{o,ext}/\kappa_o)\,(\kappa_{e,ext}/\kappa_e)$ when the optomechanical and electromechanical damping rates are matched and overwhelm the intrinsic mechanical damping rate, $\Gamma_o = \Gamma_e \gg \gamma_m$. Here, κ_o and κ_e are

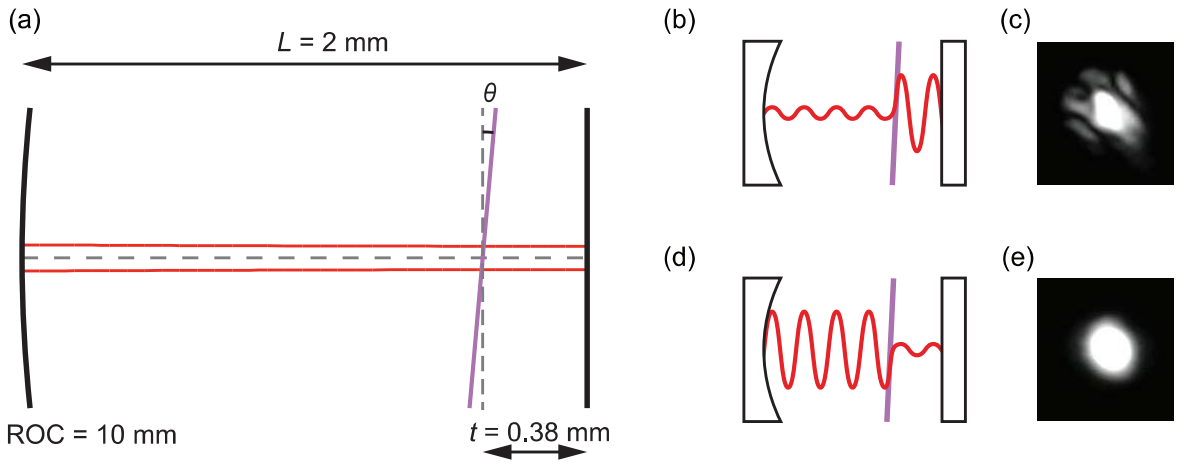

Figure 2. **Membrane misalignment.** (a) Scale drawing of representative optical cavity geometries, with cavity length $L = 2$ mm and the membrane a separation $t = 0.38$ mm from the flat mirror. Curved mirror (left black curve) with 10 mm radius of curvature (ROC) and flat mirror (right black line) confine an optical mode with $1/e^2$ radius indicated by the red curves. Cryogenic cooling can lead to angular misalignment θ of the membrane (purple line). For comparison, the optical cavity used in Ref. 23 was constructed with $L = 2.6$ mm and $t = 0.75$ mm, and that used in Refs. 24 and 25 was constructed with $L = 2.3$ mm and $t = 0.38$ mm. (b) Operating configuration of optomechanical cavity that maximizes optomechanical coupling, as the optical field (red curve) is maximized in the shorter but potentially unstable section of the cavity between the membrane and flat mirror. Membrane misalignment exaggerated for illustrative purposes. (c) Photograph of cavity mode observed operating the cavity in the configuration indicated by (b). (d) Operating configuration that has reduced optomechanical coupling but is more robust to misalignment of the membrane, because the optical mode participates less in the unstable section of the cavity between the membrane and flat mirror. (e) Photograph of the cavity mode as observed operating the cavity in more stable configuration indicated in (d).

the respective total energy loss rates of the optical cavity and LC circuit, $\kappa_{\mathrm{o,ext}}$ and $\kappa_{\mathrm{e,ext}}$ are their respective external coupling rates, and ϵ is a mode-matching factor describing the spatial overlap of the cavity mode with our signal and measurement beams. We define $\epsilon = \sqrt{\epsilon_{\mathrm{i}}\epsilon_{\mathrm{m}}}$ to describe the bidirectional efficiency, where ϵ_{i} is the mode-matching factor associated with the injected signal, and ϵ_{m} quantifies the mode matching between the measured output signal and the local oscillator used for heterodyne measurement. With our platform, we have repeatedly demonstrated efficiencies of close to 50%.[23,24]

Because the mechanical transduction mode has MHz-scale resonant frequency, it will remain highly occupied when in thermal equilibrium with the base plate of a dilution refrigerator. Optomechanical damping couples the mechanical mode to a bath with occupation $n_{\mathrm{o}} = n_{\mathrm{min,o}} + n_{\mathrm{eff,o}}$, where $n_{\mathrm{min,o}}$ is the quantum backaction limit due to imperfect sideband resolution[27] and $n_{\mathrm{eff,o}}$ is the effective optical mode occupation due to technical noise. Analogously, the occupation of the electromechanical bath is given by $n_{\mathrm{e}} = n_{\mathrm{min,e}} + n_{\mathrm{eff,e}}$. By increasing Γ_{o} and Γ_{e}, we can cool the mechanical mode below the environmental thermal occupation $n_{\mathrm{th}} = k_B T/\hbar\omega_{\mathrm{m}}$, where T is the cryostat temperature, to an equilibrium occupation $n_{\mathrm{m}} = \left(\gamma_{\mathrm{m}} n_{\mathrm{th}} + \Gamma_{\mathrm{o}} n_{\mathrm{o}} + \Gamma_{\mathrm{e}} n_{\mathrm{e}}\right)/\Gamma_{\mathrm{t}}$.

Figure 1(c) shows the displacement profile of the $\omega_m/2\pi = 1.45$ MHz mechanical mode of the membrane that we use for transduction. The capacitor pad, whose geometry is indicated by the dotted line, perturbs the mode that would otherwise have a single node line in each dimension, so we refer to it as the (2,2) mechanical mode.

Figure 1(d) is a photograph taken of a device operating at dilution-refrigerator temperatures, showing the membrane, illuminated by non-resonant light from an LED, and the cavity mode. The position of the optical mode is chosen to intersect with the antinode of mechanical motion in order to maximize optomechanical coupling.

3. MEMBRANE MISALIGNMENT

On cryogenically cooling the electro-optomechanical transducer, thermal contraction can lead to an angular misalignment θ between the membrane surface and the plane perpendicular to the axis of the optical cavity mode, illustrated in Fig. 2(a). Such misalignment negatively impacts transducer performance by coupling the

fundamental Gaussian optical mode used for transduction to more spatially distributed and lossier higher-order modes,[28] leading to inefficiency from optical loss and additional noise from sensitivity of the superconducting resonator to optical pump power. In operating the transducer device in Ref. 23, we observed higher optical cavity loss when operating in the high-optomechanical-coupling configuration that the transducer was designed for, with the optical field building up in the region between the membrane and the flat mirror (Fig. 2(b)). The transmitted optical mode in this configuration demonstrated visible hybridization with higher-order cavity modes, as shown in the photograph in Fig. 2(c).

By changing the position of the membrane relative to the optical standing wave, we operated the cavity in the more stable configuration in which the optical field builds up preferentially in the region between the curved mirror and the membrane, illustrated in Fig. 2(d). In this operating configuration, the cavity exhibited less of the undesirable loss due to misalignment, and the transmitted optical mode looked like a fundamental Gaussian mode, as shown in Fig. 2(e).

3.1 Membrane–mirror etalon

Membrane-based transducers require careful integration of the electromechanical assembly with the optical cavity. In our transducers, the electromechanical device consists of a flip-chip assembly comprised of a top chip that supports the membrane and the mechanically compliant capacitor pad, and a bottom chip that houses the remainder of the LC circuit and external coupling circuitry. Posts on the bottom chip set the capacitor spacing of hundreds of nanometers.

To make the membrane alignment within the optical cavity robust to thermal contraction, ideally the membrane and the flat cavity mirror should be integrated into a single structure, ensuring that the optical mode is always perpendicular to the membrane. We refer to this structure, in which the membrane and flat mirror are parallel, as a membrane-mirror etalon. A stiff design constraint in engineering such an etalon is that the electromechanical device, and the fragile spacing of its capacitor, must not be affected by affixing a mirror to it.

To realize an electromechanical membrane-mirror etalon, we chemically bond the flat mirror to the bottom chip of the electromechanical device, as depicted by the optomechanical cavity architecture shown in Fig. 3(a). Compared to mounting the electromechanical device separately from the optical cavity, as done in Refs. 17

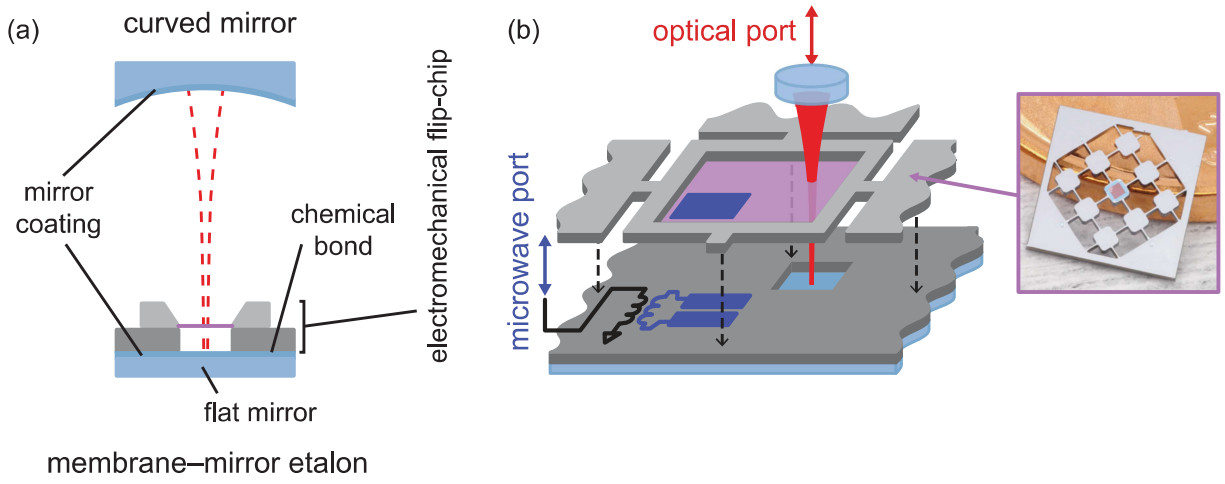

Figure 3. **Transducer with bonded membrane-mirror etalon.** (a) Diagram of optical cavity with bonded membrane-mirror etalon. The flat mirror chip (light blue) is chemically bonded to the bottom chip of the electromechanical device (dark gray), reducing the probability of misalignment between the membrane (purple line) and the mirror coating (dark blue line). (b) Illustration of transducer with bonded etalon.[24] The top chip of the electromechanical circuit is exploded upward to show schematic representation of the mechanically-compliant LC circuit (blue) and coupling circuitry (black). The optical mode (red) pierces the corner of the membrane (purple) opposite the capacitor pad. The inset photo shows the top chip of the electromechanical device that supports the membrane (false-colored purple).

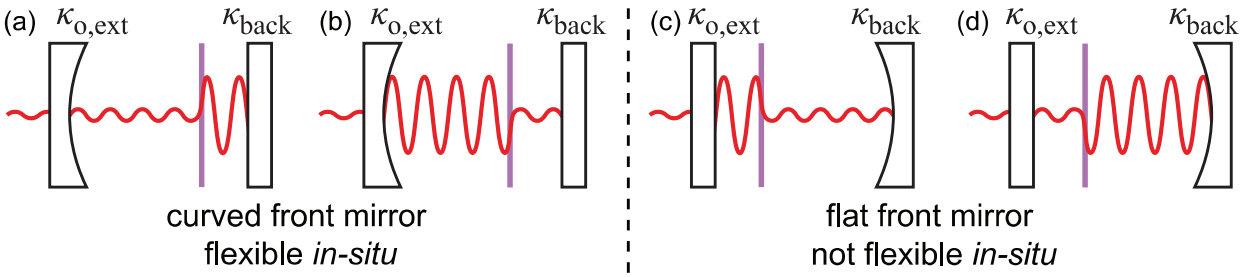

Figure 4. **Choice of front mirror.** For our cavity, we choose a front mirror mirror to have much larger external coupling than the other $\kappa_{o,ext} \gg \kappa_{back}$, to maximize $\kappa_{o,ext}/\kappa_o$. With the curved mirror chosen to be the front mirror, the cavity can be operated with the optical field predominantly building up on the shorter side of the cavity as illustrated in (a) or in the longer side of the cavity as illustrated in (b), with similar values of $\kappa_o = \kappa_{o,ext} + \kappa_{back} + \kappa_{int}$. The sideband resolution is then maintained between both operating configurations. Conversely, if the flat mirror is chosen to be the front mirror, then operating the cavity in the configuration with high optomechanical coupling (c) will have significantly greater value of κ_o than when the optical field is concentrated on the longer side of the cavity with the higher-reflectivity back mirror (d).

and 23, this reduces the effects of thermal contraction from the membrane's mounting hardware. Furthermore, the membrane does not require *in-situ* manual alignment to the optical cavity mode during assembly, as the mirror coating is now referenced to the bottom surface of the bottom chip of the electromechanical circuit, to which the optical mode will necessarily be perpendicular. Thus, in practice, optomechanical cavity alignment is limited by our ability to align the membrane to the bottom electromechanical chip, and maintain that alignment upon cryogenic cooling.

Fig. 3(b) is an illustration of the transducer schematically depicting the locations of the electromechanical circuit and optical mode. The inset photo shows the top chip of the electromechanical device. A single-unit-cell phononic filter is patterned into the silicon chip surrounding the membrane, shielding the mechanical mode from being driven by its thermal environment.

We bond the mirror using a hydrophilic Si-SiO_2 bonding process. The SiO_2-Ta_2O_5 dielectric stack that makes the high-reflectivity optical coating is deposited directly on a silicon wafer by FiveNine Optics, with a 100 Å capping layer of SiO_2 to allow chemical bonding. A 3 µm SiO_2 stress-compensation layer is deposited on the reverse side of the mirror wafer to ensure the wafer is flat during bonding. To bond wafers together, we first perform an acid clean and oxygen plasma clean to remove any contaminants. Then, we apply a hydrogen plasma and rinse the wafers in deionized water to prepare dangling hydrogen bonds. These bonds ensure that the wafers adhere to each other when initially pressed together, and a subsequent anneal at 150 °C strengthens the bond enough to withstand routine handling and thermal cycling.[29] After bonding mirror wafer to the silicon wafer housing the superconducting circuitry of the bottom chip of the electromechanical device, we remove the stress-compensation layer, in order to ensure symmetrical stress on the bonded assembly upon cryogenic cooling. We have found that the bowing that results when the stress-compensation layer is left in place is sufficient to collapse the electromechanical device, and short the mechanically compliant capacitor.

3.2 Choice of front mirror

Because the electromechanical etalon design greatly reduces thermal misalignment, it is useful to have the experimental flexibility to operate in either of the configurations illustrated in Figs. 2(b) and 2(d), in case one is more favorable for a given device. We can select between these operating configurations *in-situ* by tuning the laser wavelength to vary the position of the membrane relative to the optical standing wave.

To maximize $\kappa_{o,ext}/\kappa_o$ and transduction efficiency, we use asymmetric mirror transmissions, and label the higher-transmission, externally coupled mirror as the front mirror. In choosing a value for the front mirror transmission, there is a tension between maximizing $\kappa_{o,ext}/\kappa_o$ and maintaining the sideband resolution that determines $n_{min,o}$, which requires $\kappa_o \ll 4\omega_m$. It is desirable to make $\kappa_{o,ext}$ as large as possible to increase the likelihood it dominates $\kappa_o = \kappa_{o,ext} + \kappa_{back} + \kappa_{int}$, where κ_{back} is the rate of transmission through the back mirror, and κ_{int} is the uncontrolled contribution to κ_o from scattering and absorption in the cavity. At the same time,

κ_o must be kept sufficiently low to achieve the sideband-resolution necessary for the noise performance required of the transducer. In general, $\kappa_{o,ext}$, κ_{back}, κ_{int}, and κ_o all vary with the position of the membrane relative to the optical standing wave, as the optical mode participates more or less strongly with the mirror surfaces and lossy scatterers.

By choosing the curved mirror to be the front mirror, the optical field can build up preferentially in the shorter and higher-finesse subsection of the cavity defined by the etalon (Fig. 4(a)), or in the longer and more transmissive subsection between the curved mirror and the membrane (Fig. 4(b)). In this arrangement, because the mirror reflectivities and length of the cavity sections have competing effects on optical loss rates, changing from one operating configuration to the other maintains a similar value for κ_o, maintaining sideband resolution.

If, on the other hand, the flat mirror associated with the shorter section of the cavity were chosen to be the more transmissive front mirror, the operating configuration indicated in Fig. 4(c) would have larger κ_o than that indicated in Fig. 4(d). A choice of a specific value for the input mirror transmission to balance the constraints on sideband resolution and $\kappa_{o,ext}/\kappa_o$ would then need to account for which operating configuration would be used, committing to that mode of operation in advance.

We took advantage of the flexibility offered by our choice of front mirror when measuring the device described in Sec. 4. Though it used a bonded electromechanical etalon, we found there was additional loss associated with the etalon, and we were able to work in the configuration indicated in Fig. 4(b) in order to cool the mechanical mode to less than one phonon of occupation, operate with minimum added noise,[24] and read out the state of a superconducting qubit.[25]

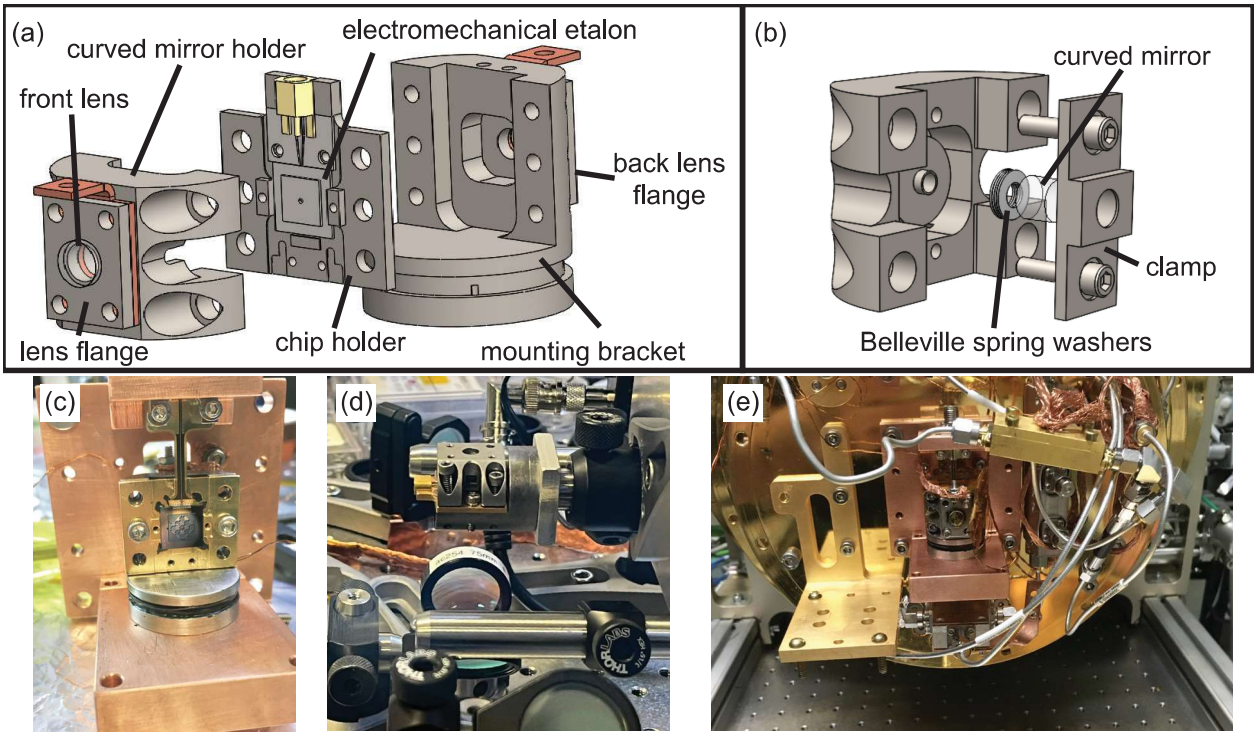

Figure 5. **Transducer cavity assembly.** (a) Computer-aided design (CAD) rendering indicating assembly of the transducer. (b) CAD rendering of curved mirror holder with Belleville spring washers clamping curved mirror substrate in place. (c) Photograph of electromechanical etalon mounted to chip holder. (d) Photograph of curved mirror installation. The chip holder is oriented horizontally so the curved mirror holder can be easily repositioned to control placement of the cavity mode. (e) Photograph of assembled transducer mounted to base plate of dilution refrigerator.

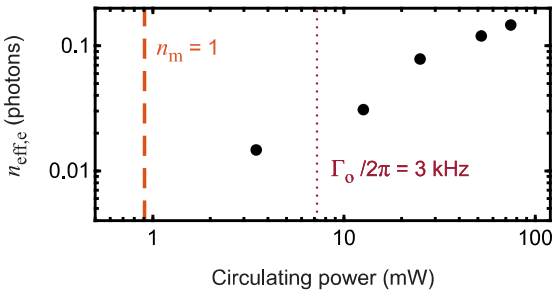

Figure 6. **Microwave circuit noise vs. optical circulating power.** The laser-induced noise remains small up to very high circulating powers.[24]

3.3 Additional details of cavity design and assembly

The computer-aided design rendering in Fig. 5(a) shows how the electromechanical etalon is integrated into an optical cavity to form the transducer device. The curved mirror holder, chip holder and mounting bracket are machined from Invar to minimize geometry changes from thermal contraction. Lenses with 18 mm focal length are mounted at the front of the optical cavity to facilitate mode matching, and at the back of the cavity in order to image the membrane and cavity mode in transmission for diagnostic information. Although the curved mirror was epoxied to the curved mirror holder for the device measured in Sec. 4, it can be clamped within the curved mirror holder using Belleville spring washers for a construction without epoxy, as shown in Fig. 5(b). Clamping cavity mirrors was found to be advantageous in another transducer platform that uses a cryogenic Fabry-Pérot cavity, one that realizes a quantum link between optical and millimeter-wave frequencies.[6,30] We note that we observe greater cavity birefringence with the clamped mounting of the mirror, presumably due to additional strain on the mirror coating. Though earlier cavity designs had piezoelectric actuators to tune the positions of the mirrors, they provided a channel for electrical noise to couple into the cavity length, and consequently the optical output of the transducer. We achieve improved transducer performance by eliminating piezoelectric actuators from the design, which requires that we use a tunable laser (Toptica CTL 1050) to bring the laser into resonance with the cavity. By addressing subsequent longitudinal cavity modes separated by the membrane perturbed free-spectral-range of the optical cavity, we can tune the position of the membrane along the optical standing wave and vary the optomechanical coupling.

Fig. 5(c) is a photograph showing the etalon mounted in the chip holder, before the curved mirror holder is installed. When installing the curved mirror holder, we use a superluminescent diode to locate the optical mode and position it close to the antinode of mechanical motion for maximum optomechanical coupling. The chip holder and curved mirror holder are oriented horizontally during assembly, as shown in Fig. 5(d), in order to achieve better control of the optical mode position on the membrane. Fig. 5(e) shows the transducer device assembled and mounted to the base plate of the dilution refrigerator.

4. EFFECTS OF CONTINUOUS OPTICAL PUMPING

Using a device with a robust optical cavity and the phononic shield, we have laser cooled the mechanical transduction mode to an occupation of less than one phonon, and achieved an input-referred added noise of 3.2 photons/s/Hz.[24] We also used the transducer to read out the state of a superconducting transmon qubit.[25] In this section, we quantify the effect of the laser pump on the microwave circuit in the transducer, and on the dephasing rate of a transmon qubit.

4.1 Low laser-induced microwave circuit noise

In contrast with other transducer platforms for which pulsing of the optical pump dramatically improves transducer performance,[18,20,31] the optical pump does not add significant noise in our platform, even under continuous operation. To quantify the effect of the optical pump, we turn off the microwave pump and measure the power spectrum emanating from the LC circuit to determine $n_{\mathrm{eff,e}}$ as a function of the optical circulating

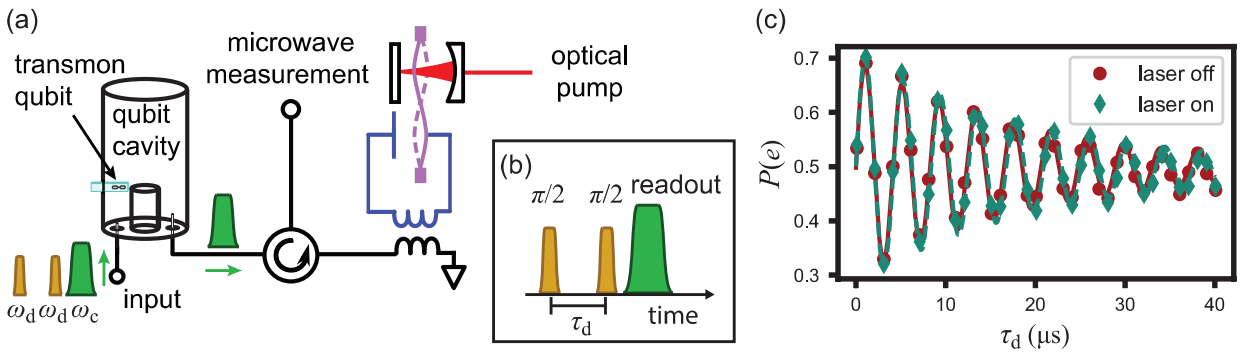

Figure 7. **Backaction on superconducting qubit.** (a) Simplified measurement setup. Qubit drive and readout pulses are injected into the qubit cavity input port. The readout pulse is transmitted through the cavity, reflects from the transducer to be measured with microwave heterodyne detection. (b) Ramsey pulse sequence. (c) Results of Ramsey experiment with laser off (red circles) and laser on (cyan diamonds), indicating no measurable effect due to the optical pump.[25]

power (Fig. 6).[24] Even at circulating powers much higher than those used in transducer operation, $n_{\mathrm{eff,e}}$ remains a fraction of a photon. Comparing the high optical circulating powers shown in Fig. 6 with powers used to operate the transducer, we cooled the mechanical mode to an occupation of 1 phonon with an optical circulating power of 900 μW, indicated by the orange dashed line. The red dotted line corresponds to an optomechanical damping rate $\Gamma_o/2\pi = 3$ kHz, which would correspond to a transduction bandwidth of $\Gamma_t/2\pi = 6$ kHz with matched electromechanical damping rate, compatible with state-of-the-art superconducting qubit lifetimes of approximately 1 ms. Even with optical powers as high as 74 mW circulating less than 300 μm from the fragile superconducting LC circuit, our robust Fabry-Pérot cavity architecture allows the superconducting circuit to operate with $n_{\mathrm{eff,e}} < 0.15$.

4.2 Low backaction on superconducting transmon qubit

After demonstrating optical readout of the transmon qubit via the transducer, we perform Ramsey experiments on the superconducting qubit to quantify the backaction on the qubit due to any unwanted photons arriving from operating the transducer.[25,32] The experimental setup is illustrated in Fig. 7(a). The transmon qubit is dispersively coupled to a three-dimensional microwave cavity, allowing dispersive readout of the qubit, in which the qubit state is encoded in the phase of a readout pulse applied at the cavity's resonant frequency ω_c.[33] The weakly-coupled input port to the qubit cavity is used to apply drive pulses to manipulate the state of the qubit at frequency ω_d, close to the qubit's resonant frequency, in addition to the readout pulses. The readout pulse containing information about the state of the qubit is then transmitted through the strongly-coupled readout port and routed toward the transducer, in order to demonstrate optical readout. Because we want to determine the backaction due to the transducer, we instead measure the readout pulse using the microwave measurement port, detecting the signal that is reflected from the transducer's microwave port, using a circulator.

To measure the coherence time T_2 of the qubit, a Ramsey sequence is applied to the qubit followed by a readout pulse, as shown in Fig. 7(b). The results of Ramsey experiments with the transducer's optical pump both off and on are shown in Fig. 7(c). We find the coherence time of the qubit when the optical pump is off to be $T_{2,\mathrm{off}} = 20.4 \pm 0.2$ μs. We then turn on the optical pump, using a circulating power of 11 mW in the Fabry-Pérot cavity in order to operate the transducer with $\Gamma_o/2\pi = 5$ kHz, the maximum optical power we used in Ref. 25. We measure $T_{2,\mathrm{on}} = 20.7 \pm 0.2$ μs, indicating that continuous operation of the transducer's optical pump has no measurable effect on the superconducting qubit. The ability to operate a transducer without causing significant backaction on the interfaced qubit is paramount for generating entanglement between two quantum registers via an optical link, and thus far demonstration of such low-backaction performance is unique to our platform.

5. CONCLUSION

Sensitivity of the transducer to optical pumping is an outstanding challenge for quantum microwave-to-optical transduction. We have described the robust and operationally flexible optical cavity architecture that allows us

to transduce with continuous laser illumination. We have shown that, in contrast with other microwave-to-optical transducer platforms, such optical pumping causes negligible impact on the transducer's microwave resonator and a connected transmon qubit. Though the necessity of a microwave pump and the MHz-scale mechanical mode frequency present challenges to membrane-based tranducers,[24] the spatial confinement of light provided by its carefully integrated Fabry-Pérot cavity is promising for the possibility of continuous quantum transduction, which would be beneficial for communication rates in a network of superconducting quantum computers.

ACKNOWLEDGMENTS

We thank Kim Hagen, Hans Green, Kyle Thatcher, Adam Ellzey, Calvin Schwadron, Terry Brown, Ramin Lalezari, Peter Burns, and Andrew Higginbotham for their technical assistance and helpful discussions. This work was supported by funding from ARO Grant W911NF2310376, NSF Grant No. PHY-2317149, NSF QLCI Award OMA - 2016244, and the Baur-SPIE Endowed Chair at JILA.

REFERENCES

[1] Teoh, J. D., Winkel, P., Babla, H. K., Chapman, B. J., Claes, J., de Graaf, S. J., Garmon, J. W. O., Kalfus, W. D., Lu, Y., Maiti, A., Sahay, K., Thakur, N., Tsunoda, T., Xue, S. H., Frunzio, L., Girvin, S. M., Puri, S., and Schoelkopf, R. J., "Dual-rail encoding with superconducting cavities," *Proceedings of the National Academy of Sciences* **120**, e2221736120 (Oct. 2023).

[2] Liao, S.-K., Cai, W.-Q., Handsteiner, J., Liu, B., Yin, J., Zhang, L., Rauch, D., Fink, M., Ren, J.-G., Liu, W.-Y., Li, Y., Shen, Q., Cao, Y., Li, F.-Z., Wang, J.-F., Huang, Y.-M., Deng, L., Xi, T., Ma, L., Hu, T., Li, L., Liu, N.-L., Koidl, F., Wang, P., Chen, Y.-A., Wang, X.-B., Steindorfer, M., Kirchner, G., Lu, C.-Y., Shu, R., Ursin, R., Scheidl, T., Peng, C.-Z., Wang, J.-Y., Zeilinger, A., and Pan, J.-W., "Satellite-Relayed Intercontinental Quantum Network," *Physical Review Letters* **120**, 030501 (Jan. 2018).

[3] Verdú, J., Zoubi, H., Koller, C., Majer, J., Ritsch, H., and Schmiedmayer, J., "Strong Magnetic Coupling of an Ultracold Gas to a Superconducting Waveguide Cavity," *Physical Review Letters* **103**, 043603 (July 2009).

[4] Hafezi, M., Kim, Z., Rolston, S. L., Orozco, L. A., Lev, B. L., and Taylor, J. M., "Atomic interface between microwave and optical photons," *Physical Review A* **85**, 020302 (Feb. 2012).

[5] Covey, J. P., Sipahigil, A., and Saffman, M., "Microwave-to-optical conversion via four-wave mixing in a cold ytterbium ensemble," *Physical Review A* **100**, 012307 (July 2019).

[6] Kumar, A., Suleymanzade, A., Stone, M., Taneja, L., Anferov, A., Schuster, D. I., and Simon, J., "Quantum-enabled millimetre wave to optical transduction using neutral atoms," *Nature* **615**, 614–619 (Mar. 2023).

[7] Imamoğlu, A., "Cavity QED Based on Collective Magnetic Dipole Coupling: Spin Ensembles as Hybrid Two-Level Systems," *Physical Review Letters* **102**, 083602 (Feb. 2009).

[8] Marcos, D., Wubs, M., Taylor, J. M., Aguado, R., Lukin, M. D., and Sørensen, A. S., "Coupling Nitrogen-Vacancy Centers in Diamond to Superconducting Flux Qubits," *Physical Review Letters* **105**, 210501 (Nov. 2010).

[9] Bartholomew, J. G., Rochman, J., Xie, T., Kindem, J. M., Ruskuc, A., Craiciu, I., Lei, M., and Faraon, A., "On-chip coherent microwave-to-optical transduction mediated by ytterbium in YVO4," *Nature Communications* **11**, 3266 (June 2020).

[10] Ilchenko, V. S., Savchenkov, A. A., Matsko, A. B., and Maleki, L., "Whispering-gallery-mode electro-optic modulator and photonic microwave receiver," *JOSA B* **20**, 333–342 (Feb. 2003).

[11] Xiong, C., Pernice, W. H. P., and Tang, H. X., "Low-Loss, Silicon Integrated, Aluminum Nitride Photonic Circuits and Their Use for Electro-Optic Signal Processing," *Nano Letters* **12**, 3562–3568 (July 2012).

[12] Rueda, A., Sedlmeir, F., Collodo, M. C., Vogl, U., Stiller, B., Schunk, G., Strekalov, D. V., Marquardt, C., Fink, J. M., Painter, O., Leuchs, G., and Schwefel, H. G. L., "Efficient microwave to optical photon conversion: an electro-optical realization," *Optica* **3**, 597–604 (June 2016).

[13] Fan, L., Zou, C.-L., Cheng, R., Guo, X., Han, X., Gong, Z., Wang, S., and Tang, H. X., "Superconducting cavity electro-optics: A platform for coherent photon conversion between superconducting and photonic circuits," *Science Advances* **4**, eaar4994 (Aug. 2018).

[14] Hease, W., Rueda, A., Sahu, R., Wulf, M., Arnold, G., Schwefel, H. G., and Fink, J. M., "Bidirectional Electro-Optic Wavelength Conversion in the Quantum Ground State," *PRX Quantum* **1**, 020315 (Nov. 2020).

[15] Bochmann, J., Vainsencher, A., Awschalom, D. D., and Cleland, A. N., "Nanomechanical coupling between microwave and optical photons," *Nature Physics* **9**, 712–716 (Nov. 2013).

[16] Balram, K. C., Davanço, M. I., Song, J. D., and Srinivasan, K., "Coherent coupling between radiofrequency, optical and acoustic waves in piezo-optomechanical circuits," *Nature Photonics* **10**, 346–352 (May 2016).

[17] Andrews, R. W., Peterson, R. W., Purdy, T. P., Cicak, K., Simmonds, R. W., Regal, C. A., and Lehnert, K. W., "Bidirectional and efficient conversion between microwave and optical light," *Nature Physics* **10**, 321–326 (Apr. 2014).

[18] Mirhosseini, M., Sipahigil, A., Kalaee, M., and Painter, O., "Superconducting qubit to optical photon transduction," *Nature* **588**, 599–603 (Dec. 2020).

[19] Meesala, S., Lake, D., Wood, S., Chiappina, P., Zhong, C., Beyer, A. D., Shaw, M. D., Jiang, L., and Painter, O., "Quantum entanglement between optical and microwave photonic qubits," (Dec. 2023).

[20] Sahu, R., Hease, W., Rueda, A., Arnold, G., Qiu, L., and Fink, J. M., "Quantum-enabled operation of a microwave-optical interface," *Nature Communications* **13**, 1276 (Mar. 2022).

[21] Sahu, R., Qiu, L., Hease, W., Arnold, G., Minoguchi, Y., Rabl, P., and Fink, J. M., "Entangling microwaves with light," *Science* **380**, 718–721 (May 2023).

[22] Regal, C. A. and Lehnert, K. W., "From cavity electromechanics to cavity optomechanics," *Journal of Physics: Conference Series* **264**, 012025 (Jan. 2011).

[23] Higginbotham, A. P., Burns, P. S., Urmey, M. D., Peterson, R. W., Kampel, N. S., Brubaker, B. M., Smith, G., Lehnert, K. W., and Regal, C. A., "Harnessing electro-optic correlations in an efficient mechanical converter," *Nature Physics* **14**, 1038–1042 (Oct. 2018).

[24] Brubaker, B., Kindem, J., Urmey, M., Mittal, S., Delaney, R., Burns, P., Vissers, M., Lehnert, K., and Regal, C., "Optomechanical Ground-State Cooling in a Continuous and Efficient Electro-Optic Transducer," *Physical Review X* **12**, 021062 (June 2022).

[25] Delaney, R. D., Urmey, M. D., Mittal, S., Brubaker, B. M., Kindem, J. M., Burns, P. S., Regal, C. A., and Lehnert, K. W., "Superconducting-qubit readout via low-backaction electro-optic transduction," *Nature* **606**, 489–493 (June 2022).

[26] Aspelmeyer, M., Kippenberg, T. J., and Marquardt, F., "Cavity optomechanics," *Reviews of Modern Physics* **86**, 1391–1452 (Dec. 2014).

[27] Peterson, R., Purdy, T., Kampel, N., Andrews, R., Yu, P.-L., Lehnert, K., and Regal, C., "Laser Cooling of a Micromechanical Membrane to the Quantum Backaction Limit," *Physical Review Letters* **116**, 063601 (Feb. 2016).

[28] Sankey, J. C., Yang, C., Zwickl, B. M., Jayich, A. M., and Harris, J. G. E., "Strong and tunable nonlinear optomechanical coupling in a low-loss system," *Nature Physics* **6**, 707–712 (Sept. 2010).

[29] Plößl, A. and Kräuter, G., "Wafer direct bonding: tailoring adhesion between brittle materials," *Materials Science and Engineering: R: Reports* **25**, 1–88 (Mar. 1999).

[30] Stone, M., *Hybrid Cavity QED with Rydberg Atoms*, PhD Thesis, University of Chicago (2021).

[31] Meesala, S., Wood, S., Lake, D., Chiappina, P., Zhong, C., Beyer, A. D., Shaw, M. D., Jiang, L., and Painter, O., "Non-classical microwave-optical photon pair generation with a chip-scale transducer," (Mar. 2023).

[32] Hatridge, M., Shankar, S., Mirrahimi, M., Schackert, F., Geerlings, K., Brecht, T., Sliwa, K. M., Abdo, B., Frunzio, L., Girvin, S. M., Schoelkopf, R. J., and Devoret, M. H., "Quantum Back-Action of an Individual Variable-Strength Measurement," *Science* **339**, 178–181 (Jan. 2013).

[33] Blais, A., Huang, R.-S., Wallraff, A., Girvin, S. M., and Schoelkopf, R. J., "Cavity quantum electrodynamics for superconducting electrical circuits: An architecture for quantum computation," *Physical Review A* **69**, 062320 (June 2004).